



FULL LENGTH ARTICLE

Tsc2 mutation induces renal tubular cell nonautonomous disease

Prashant Kumar^{a,b,1}, Fahad Zadjali^{a,b,c,1}, Ying Yao^{a,b}, Daniel Johnson^d, Brian Siroky^b, Aristotelis Astrinidis^a, Peter Vogel^e, Kenneth W. Gross^f, John J. Bissler^{a,b,g,*}

^a Department of Pediatrics, University of Tennessee Health Science Center and Le Bonheur Children's Hospital, Memphis, TN 38103, USA

^b Children's Foundation Research Institute (CFRI), Le Bonheur Children's Hospital, Memphis, TN 38105, USA

^c Department of Clinical Biochemistry, College of Medicine & Health Sciences, Sultan Qaboos University, Muscat 123, Oman

^d Molecular Bioinformatics Center, University of Tennessee Health Science Center, Memphis, TN 38163, USA

^e Department of Veterinary Pathology, St. Jude Children's Research Hospital, Memphis, TN 38105, USA

^f Department of Molecular and Cellular Biology, Roswell Park Comprehensive Cancer Center, Buffalo, NY 14263, USA

^g Pediatric Medicine Department, St. Jude Children's Research Hospital, Memphis, TN 38105, USA

Received 11 November 2020; received in revised form 25 March 2021; accepted 31 March 2021
Available online 27 April 2021

KEYWORDS

Cell nonautonomous trait;
Polycystic kidney disease;
Renal cystogenesis;
Tuberous sclerosis complex

Abstract TSC renal cystic disease is poorly understood and has no approved treatment. In a new principal cell-targeted murine model of *Tsc* cystic disease, the renal cystic epithelium is mostly composed of type A intercalated cells with an intact *Tsc2* gene confirmed by sequencing, although these cells exhibit a *Tsc*-mutant disease phenotype. We used a newly derived targeted murine model in lineage tracing and extracellular vesicle (EV) characterization experiments and a cell culture model in EV characterization and cellular induction experiments to understand TSC cystogenesis. Using lineage tracing experiments, we found principal cells undergo clonal expansion but contribute very few cells to the cyst. We determined that cystic kidneys contain more interstitial EVs than noncystic kidneys, excrete fewer EVs in urine, and contain EVs in cyst fluid. Moreover, the loss of *Tsc2* gene in EV-producing cells greatly changes the effect of EVs on renal tubular epithelium, such that the epithelium develops increased secretory and proliferative pathway activity. We demonstrate that the mTORC1

* Corresponding author. Chief of Nephrology, Department of Pediatrics, UTHSC, and Medical Director of Nephrology, St. Jude Children's Research Hospital, 51N. Dunlap St., Memphis, TN 38103, USA.

E-mail address: jbissler@uthsc.edu (J.J. Bissler).

Peer review under responsibility of Chongqing Medical University.

¹ These authors contributed equally to this work.

pathway activity is independent from the EV production, and that the EV effects for a single cell line can vary significantly. TSC cystogenesis involves significant contribution from genetically intact cells conscripted to the mutant phenotype by mutant cell derived EVs.

Copyright © 2021, Chongqing Medical University. Production and hosting by Elsevier B.V. This is an open access article under the CC BY-NC-ND license (<http://creativecommons.org/licenses/by-nc-nd/4.0/>).

Introduction

During renal development, collecting duct cells arise from the ureteric bud tip, and these progenitor collecting duct cells differentiate into principal and intercalated cells.¹ Later in life, these collecting duct cells exhibit significant plasticity, and intercalated cells can contribute to extracellular fluid volume regulation by NaCl transepithelial transport to facilitate intravascular volume protection with principal cells (reviewed by Eladari et al²). The relative number and activity of type A and type B intercalated cells are regulated by mechanisms that include interconversion between the two subtypes to affect systemic acid–base balance.^{3,4} Carbonic anhydrase II is critical for the function of both subtypes, and genetic loss of this enzyme leads to depletion of intercalated cells and a proportional increase in aquaporin 2-expressing principal cells.⁵ Cortical collecting duct cell plasticity also extends to the ratio of intercalated cells to principal cells.^{6,7} Potassium homeostasis is affected by principal cells that secrete and intercalated cells that absorb potassium. Cell lineage tracing experiments with potassium depletion revealed intercalated-principal cell interconversion in the medullary collecting duct.⁸ Lithium, through Notch and Foxi1 pathways, can increase the percentage of intercalated cells.^{6,9–11}

Cortical collecting duct adaption to environmental conditions uses EVs as an intercellular communication system. Both *in vivo* and *in vitro* renal collecting duct cells release EVs that contain aquaporin-2, and desmopressin in both systems significantly increased aquaporin-2 in EVs.¹² These isolated aquaporin-2-containing EVs induce cortical collecting duct cells that have not been exposed desmopressin to conduct water.¹² Interestingly, desmopressin increased uptake of EVs in cortical collecting duct cells *in vivo* and *in vitro*,¹³ and this effect is suppressed by selective V2 receptor inhibition using tolvaptan.¹³

While such cellular plasticity is a mechanism for adaption and survival, the mechanism may be conscripted to cause disease. We recently showed a targeted *Tsc2* disruption in murine renal tubular principal cells induced a *Tsc*-mutant renal polycystic disease phenotype composed of type A intercalated cells that maintained an intact *Tsc2* gene confirmed by sequencing,¹⁴ and that the loss of *Tsc2* function increases EV production.¹⁵ Using a novel mouse model and cell culture systems in lineage tracing experiments we demonstrate in this manuscript that EVs from mutant principal cells conscript *Tsc2*-expressing intercalated cells to adopt a *Tsc2*-mutant

disease phenotype resulting in a cell nonautonomous cystic phenotype.

Materials and methods

Reagents

Lithium chloride (Cat# 310,468, molecular weight 42.39), cobalt chloride (Cat# C-2644, molecular weight 237.9) and rapamycin were purchased from Sigma Aldrich (St. Louis, MO). The following primary antibodies were used for the Western blots: rabbit anti-CD63 (1:500, Proteintech 25682-1-AP, Rosemont, IL), rabbit anti-CD81 (1:1000, sc-18877), rabbit anti-ARL13b (1:1000, ab83879), mouse anti- α CD9 (1:500, Thermo 14-0091-82, Waltham, MA), mouse anti-Alix (1:100, Proteintech 12422-1-AP), mouse anti-TSG101 (1:1000, sc-7964), rabbit anti-Pax8 (1:100, Sigma–Aldrich, AV48088, St. Louis, MO) anti-phospho-P70S6Kinase (1:5000, Cell Signaling, 9205, Danvers, MA), and total S6 (1:1000, Cell Signaling, 2317S). T-PER™ Tissue Protein Extraction Reagent used for the tissue homogenization was purchased from Thermo Scientific™ (Cat# 78510).

Generation of *Tsc2* KO mice (*Aqp2CreTsc2^{fl/fl}*) and *Aqp2CreTsc2^{fl/fl}/Confetti* mice

Floxed *Tsc2* mice (stock #027458), *AqpCre* mice (stock # 006881) and “Confetti” mice (stock #017492) were obtained from The Jackson Laboratory (Bar Harbor, ME). The “Confetti” reporter uses the Brainbow2.1 cassette inserted into the Rosa26 locus, where it is driven by the strong CAGG promoter. The reporter system is activated by excision of a floxed stop sequence by Cre recombinase. The Brainbow reporter cassette contains two inverted repeats of fluorescent reporter genes: GFP paired with inverted YFP and RFP paired with inverted CFP. The loxP sites within the construct are in direct and inverted orientations to facilitate loss of the floxed stop module and expression of one of the reporter pairs. The remaining reporter pair can continue to “flip” into the active orientation for one of the two inverted reporters while Cre activity remains present, resulting in bi-colored cells, and will be locked into one or the other orientation when Cre activity stops.¹⁶ All animal research was done in adherence to the NIH Guide for the Care and Use of Laboratory Animals. These mice were crossed to generate offspring that were heterozygous for the floxed allele and were either heterozygous or WT at the Cre allele. These mice were then intercrossed to generate

knockout mice (*Aqp2CreTsc2^{fl/fl}*, *Aqp2CreTsc2^{fl/fl}/Confetti*) and WT mice (*Aqp2Cre/Confetti*). Primers used to genotype were as follows, TSC2 Primer: Forward: ACA ATG GGA GGC ACA TTA CC, Reverse: AAG CAG GTC TGC AGT G; Cre Primer: Forward: GCA TTA CCG GTC GAT GCA ACG AGT GA, Reverse: GAG TGA ACG AAC CTG GTC GAA ATC AG; Confetti Primer: Forward common: CTC TGC CTC CTG GCT TCT, WT reverse: CGA GGC GGA TCA CAA GCA ATA, CAG promoter reverse (mutant): TCA ATG GGC GGG GGT CGT T.

DBA staining

The kidneys from knockout mice and WT mice were fixed in 10% formalin and embedded in paraffin. Tissue blocks were cut into 8- μ m-thick sections. Immunohistochemical stains were carried out using a VECTASTAIN[®] Elite[®] ABC HRP Kit (Vector Laboratories, Burlingame, CA) with 3,3-diaminobenzidine (DAB) as the chromogen (Vector Laboratories). Biotinylated DBA (Vector Laboratories, B-1035) was used at 1:300. All the sections were counterstained with Gill II Hematoxylin (Fisher Scientific, Hampton, NH). In every case, formalin-fixed tissue was subjected to heat-induced antigen retrieval. Endogenous peroxidase activity was blocked with 3% H₂O₂. An Avidin/Biotin Blocking Kit (Vector Laboratories) was used to block all endogenous biotin, biotin receptors, and avidin-binding sites present in tissues.

Cell culture

The parent renal principal cell, i.e. mIMCD, and mIMCD cells with *Tsc2* deletion (referred to as T2J) were supplemented with DMEM/F12 and 10% fetal bovine serum plus 1% penicillin-streptomycin (Invitrogen, Eugene, OR). The T2J cells were constructed by knocking out the *Tsc2* gene via the CRISPR/CAS9 gene editing method by targeting exon 4 of the *Tsc2* gene.¹⁴ Cells were starved with conditioned media containing DMEM/F12 and penicillin-streptomycin prior to the experiment. Cultures were maintained in a humidified 95% air and 5% CO₂ atmosphere at 37 °C.

EV isolation by size exclusion chromatography

EVs were isolated from three different sources such as mouse kidney cyst fluid, urine and kidney interstitials according to the protocol for a size exclusion chromatography column (SEC) (Izon Science, New Zealand). Different strategies were used to load the final sample on the SEC column.

Mouse kidney cyst fluid: We observed 19- to 21-week-old *Aqp2CreTsc2^{fl/fl}* mice for the presence of renal cysts and sacrificed the mice under terminal anesthesia with isoflurane. Under terminal anesthesia, the abdominal cavity was opened, and both kidneys were isolated and immediately processed for the collection of fluid from renal cysts. Cyst fluids were aspirated from 31G insulin syringes and collected in 1.5 ml microfuge tube.

Mouse urine: *Aqp2CreTsc2^{fl/fl}* and WT mice were individually placed in a plastic container with a wire cage lid. On the top of lid, we placed a mouse by holding the tail and

pressed gently on the lower back. The excreted urine was aspirated using a micropipette.

Kidney interstitial fluid: We anesthetized 19- to 21-week-old *Aqp2CreTsc2^{fl/fl}* (*Tsc2* KO) and WT mice using isoflurane. Kidneys were harvested immediately and processed. Kidneys were homogenized using T-PER Reagent in a ratio of 1:20 (tissue:reagent, w/v). The homogenized mixture was centrifuged at 1200 g for 15 min to pellet cells and debris. The supernatant was collected and processed further. All samples were stored at 4 °C for immediate use or at -80 °C for later use.

After all three types of samples were obtained, they were centrifuged at 2000 g for 15 min at 4 °C to remove the cell debris. Then, samples containing EVs were loaded on the top of an SEC column, and EVs were eluted as per the manufacturer's protocol.

Characterization of EVs

EVs were characterized by three different sources: tunable resistive pulse sensing (TRPS), dynamic light scattering (DLS) and transmission electron microscopy (TEM). TRPS: EVs were first analysed using TRPS by a qNano gold instrument (Izon Science). The machine was calibrated using polystyrene beads supplied by the manufacturer. EV samples were subjected to a pass through nanopore NP150 (70–420) at stretch of 47 nm under the influence of a positive voltage of 0.32 mV and pressure of 15 mbar. A minimum 500 blockade duration was counted and recorded. The data were processed and analyzed using Izon Control Suite v3.0. DLS: EVs were further characterized for size distribution using DLS, which is based on the Brownian motion of dispersed particles. Briefly, for DLS, a 50 μ L sample was homogenized with 950 μ L particle-free water. Data were recorded using Zetasizer Nano-ZS (Malvern Instruments, UK). Morphological analyses were performed using TEM. Samples were prepared using negative staining. For sample preparation, 7–8 μ L of fresh EV samples were dried on a 200 mesh Formvar/Carbon-coated grid for 25 min at room temperature. The grids were stained using 2% uranyl acetate followed by washing with PBS to remove excess staining. The grids were visualized at 59 kV using JEOL 2000EXII TEM (JEOL, Peabody, MA; access provided by the Neuroscience Institute at The University of Tennessee Health Science Center).

Western blot analysis

To analyze EV-associated markers, a maximum volume of EV suspension was used for Western blotting. Cell lysates were analyzed for total protein concentrations using Bradford protein estimation methods. Total protein (8 μ g) from control and treatments was loaded on 4%–20% Mini-PROTEAN[®] TGX[™] Precast Protein Gels (Bio-Rad Cat #456–1097 Hercules, CA). Proteins were transferred electrophoretically onto a polyvinylidene difluoride (PVDF) membrane. The membrane was blocked in 5% w/v nonfat dry milk or 5% w/v BSA for 1 h at room temperature. After blocking, the membrane was incubated with suitable primary antibodies for 16 h at 4 °C, followed by incubation

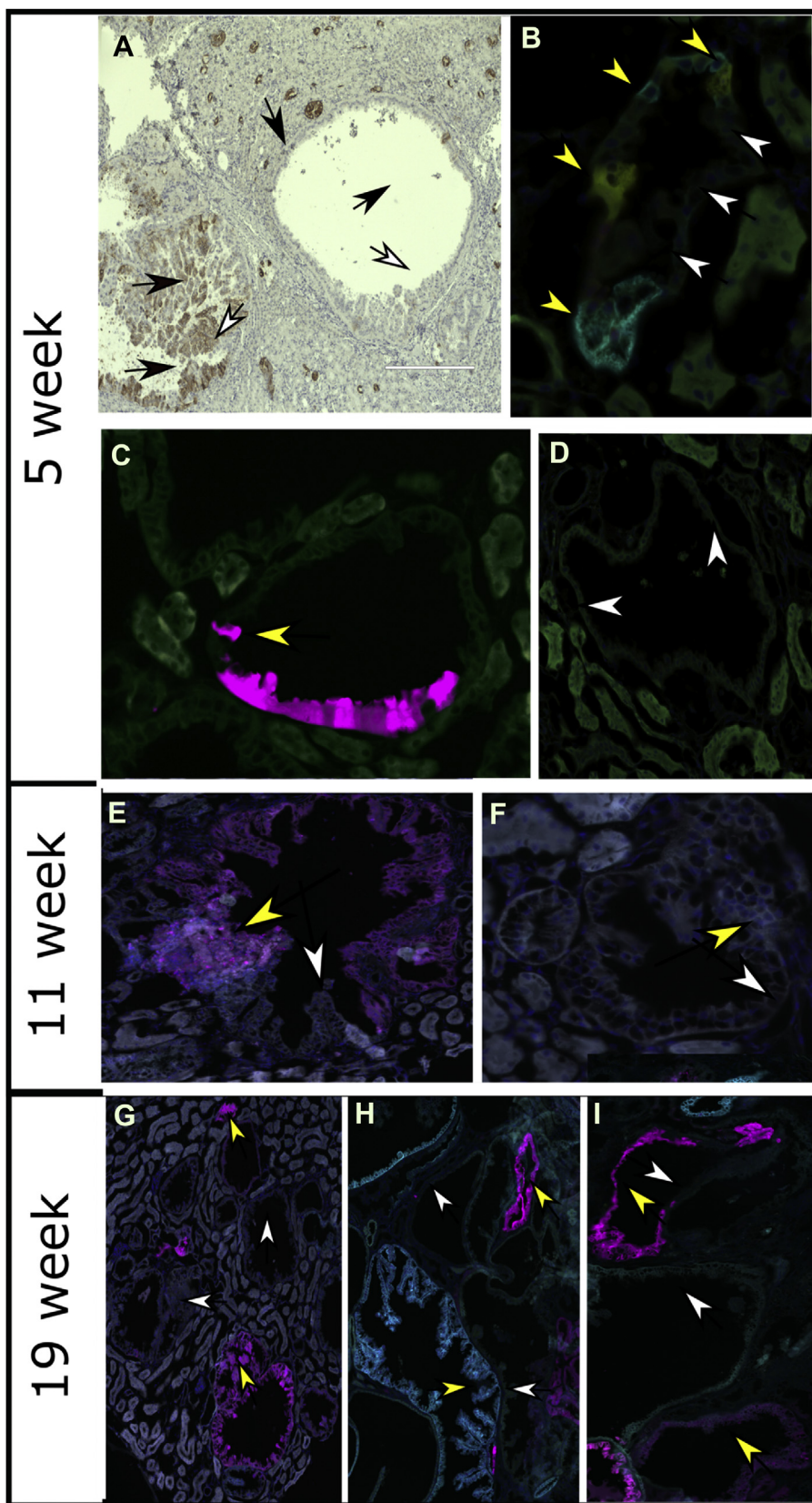


Figure 1 *Aqp2CreTsc2^{fl/fl}Confetti* cystic lesions comprise genetically normal and recombined cells. Images are divided by age of *Aqp2CreTsc2^{fl/fl}Confetti* mouse. (A) Black arrows indicate cells positive for *Dolichos biflorus* agglutinin (DBA) staining, and white arrows identify cells negative for DBA. For b-i, nuclei are stained blue; yellow arrows indicate cells that have had active Cre recombinase, and white arrows depict cells that have not turned on Cre recombinase. (B) At 5 weeks of age, cysts are microscopic.

with respective secondary antibodies. The blot was developed using a chemiluminescence reagent.

Microarray data analysis

A total of 5×10^6 M1 cells were treated with 50×10^6 EVs for 24 h. RNA was extracted by using an RNeasy kit followed by generation of cDNA. The cDNA was transcribed using an Affymetrix GeneChip expression kit.

DNased total RNA (200 ng) was amplified, fragmented, and labeled using an Affymetrix WT Plus Reagent Kit (Life Technologies Cat# 902280, Carlsbad, CA) according to Affymetrix protocols. cDNA (5500 ng) was hybridized to the array according to the manufacturer's protocol. Arrays were then washed and stained on Affymetrix Fluidics Station 450 according to the manufacturer's protocol. Arrays were scanned on a GC53000 scanner. Data were normalized and annotated using an Affymetrix Expression Console.

CSV files were retrieved from the UTHSC Molecular Resource Center after normalization performed by the Affymetrix Expression Console. Quality assurance was checked against reference probes to ensure the quality of the data. Gene names, accession numbers, and expression were mined from each text file for each sample. All non-annotated information was removed from the file, leaving only annotated probe set expression. Welch's *t* test was run for pairwise interactions to obtain *P* values for significance. Only probe sets with $P < 0.05$ were considered significant. The mean, variance, standard deviation, standard error, coefficient of variance, and fold change were calculated for each pairwise comparison. The Benjamini-Hochberg false discovery rate method was applied to obtain the adjusted *p* value for each probe set. Only probe sets with an adjusted $P < 0.05$ were considered significant. The differential gene list was loaded onto the iPathway Guide for pathway analysis. Gene set enrichment analysis was performed to validate pathway results.

Cobalt chloride, lithium chloride and rapamycin effects on EV production *in vitro*

To manipulate the production of EVs *in vitro*, cobalt chloride, lithium chloride and rapamycin were used. Cobalt chloride was used to mimic hypoxia. Briefly, an equal number of mIMCD and T2J cells were grown up to 75–80% confluency in a T75 flask containing complete DMEM/F12 medium with 10% fetal bovine serum. The cells were washed twice with sterile PBS, and the media were replaced with serum-starved DMEM/F12 media mixed with cobalt chloride,¹⁷ lithium chloride¹⁸ and rapamycin¹⁹ with a final concentration of 100 μ M, 20 nM and 20 nM, respectively, for 24 h. The culture

media were collected and processed for EV isolation and quantification according to the protocol.¹⁴

Rapamycin effects on EV production *in vivo*

For the injection experiments *in vivo*, rapamycin was first dissolved in absolute ethanol to 20 mg/ml. The vehicle solution (5.2% PEG400/5.2% Tween-80) was prepared by mixing 2.08 g of both Tween 80 and PEG400 in 50 ml water, which was then filter sterilized by Steriflip. Rapamycin (5 μ l of 20 mg/ml) was mixed with 1 ml vehicle solution to obtain a final concentration of 0.1 mg/ml. A drug solution (1 mg/kg rapamycin) was injected at 10 μ l/g body weight via the intraperitoneal route. The drug was injected twice a week for two weeks. Mice were sacrificed 24 h after the final dose. Kidneys were collected and processed for EV isolation from cyst fluid and interstitial fluid.

Results

Lineage tracing reveals conscription of normal cells in cyst and papillary lesions

We previously used a targeted murine principal cell *Tsc2* deletion model in immunofluorescence, immunohistochemistry and DNA sequencing experiments. We found that the renal cysts in the model and in patient samples were mostly comprised of type A intercalated cells with an intact *Tsc2* gene.¹⁴ The cystic incorporation of genetically intact intercalated cells was compatible with diminished *Dolichos biflorus* agglutinin (DBA) staining, which identifies principal cells.²⁰ We previously observed that cystic DBA staining could be quite variable such that some cysts and lesions could have significant staining, and some would have very little staining.¹⁴ This lack of DBA staining and intact *Tsc2* gene by sequencing in the cystic epithelium supports the possible engagement of genetically intact intercalated cells in the phenotype (Fig. 1A). Because collecting duct cell types exhibit such plasticity and can interconvert,²¹ the loss of *Tsc2* gene function could simply change the gene expression profile and turn off the principal cell phenotype, making the cell more like the parental ureteric bud/collecting duct cell and not express the proper glycosylation for DBA staining, but this would not explain the lack of genetic recombination previously identified.¹⁴ To elucidate the mechanism for these findings, we performed principal cell lineage tracing experiments by breeding *Aqp2CreTsc2^{fl/fl}* onto the Confetti mouse reporter system. This approach confers the capacity to infer individual cell fate decisions.

Because this murine model exhibits worsening cystic disease with age as occurs patients with TSC2 mutations,

Yellow arrows identify recombined cells in a microscopic cyst, white arrows denote cells that have not undergone recombination. (C) Yellow arrows identify recombined cells. Note the cells are the same color, indicating clonal expansion. (D) White arrows indicate that the section of cyst consists entirely of non-recombined cells. Cysts are three dimensional, so cells outside of the plane of the section may be recombined. (E) White arrows point to a microscopic papillary lesion within a cyst that is not recombined. Within the same cyst, another papillary lesion (yellow arrow) that has undergone recombination and clonal expansion. (F) Cyst with papillary lesion involving recombined cells (yellow arrows) and cells without recombination (white arrow). (G) Microscopic cysts with papillary lesions with recombination (yellow arrows) and papillary and cystic lesions with minimal recombination. (H) Juxtaposed papillary cystic lesions that on one side has undergone recombination adjacent to similar lesion that has not. (I) Additional macroscopic cysts comprising both recombined and nonrecombined cells.

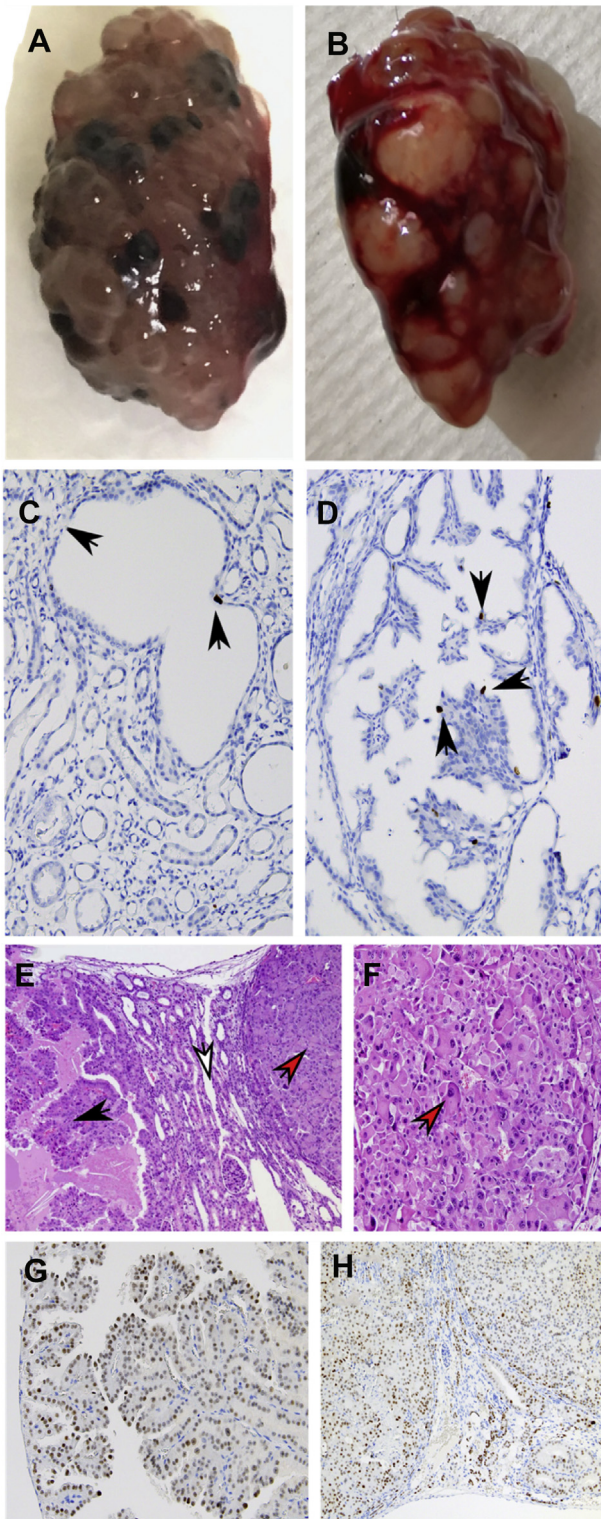


Figure 2 *Aqp2CreTsc2^{fl/fl}* mouse kidneys develop more papillary lesions with age. (A) 19 week old kidney with clear macroscopic cortical cystic disease. (B) 25 week old mouse kidney with more cysts. (C, D) Phospho-Histone-3 staining of 19-week-old *Aqp2CreTsc2^{fl/fl}Confetti* mouse kidney. (C) Black arrows indicate nuclei with positive staining for phosphorylated histone 3, a marker of active cell division in a cystic lesion. (D) Black arrows denote dividing cells in an intracystic

we examined *Aqp2CreTsc2^{fl/fl}/Confetti* kidneys at different ages. Multispectral imaging of *Aqp2CreTsc2^{fl/fl}/Confetti* kidney cysts reveals both *Tsc2* expressing and non-expressing cells and that microscopic cystic structures can be identified at 5 weeks of age (Fig. 1B). Even at this young age, which lacks an overtly macrocystic phenotype, *Tsc2*-deleted cells exhibit clonal expansion as the colors expressed are either all the same or from the same pair of fluorescent reporter genes (Fig. 1C). By 11 weeks, microscopic and macroscopic cysts can be identified that do not exhibit Cre-mediated recombination (Fig. 1D). Because cysts are three dimensional structures, the plane of the section likely determines the number of recombined cells identified. By 11 weeks, some cysts begin to show papillary lesions that may exhibit fluorescence, suggesting recombination, but also have cystic lining cells that have no evidence of recombination (Fig. 1E, F). By 19 weeks, macroscopic cysts exhibit this same theme. Cysts exhibit similar cellular phenotypes but do not appear to be only comprised of recombined cells (Fig. 1G–I). Cysts that demonstrate significant clonal expansion (Fig. 1H, I) can be immediately adjacent to cysts that do not exhibit any recombination, while both exhibit the papillary lesions.

Cystic epithelium exhibit increased cell division

While 19 week old mice exhibit macroscopic fluid filled cysts on the kidney surface (Fig. 2A) the slow but continued proliferation results in visible cellular components for those rare mice that can reach 25 weeks of age (Fig. 2B). Using phosphorylated histone 3 to identify dividing cells,^{22–24} the overall proliferation of the cysts and papillary lesions are qualitatively similar (Fig. 2C, D). These papillary lesions in the *Aqp2CreTsc2^{fl/fl}* mouse can go on to exhibit papillary renal cell carcinoma lesions by certified veterinarian pathological review (Fig. 2E). The lesions can even exhibit renal cell carcinoma with rhabdoid features (Fig. 2F). Both the proliferative lesions, the adenomatous hyperplasia of the cyst lining (Fig. 2G), and the renal cell carcinoma (Fig. 2H) express Pax8. These results raise the question of how normal cells are being conscripted into the pathological process.

Cystic kidneys contain more interstitial EVs than normal kidneys

EVs play an important role in development,²⁵ renal physiology,^{26,27} abnormal proliferation, and renal cancer.^{28–31} Additionally, cysts can contain very few mutant cells. We posited that the *Tsc2*-mutant kidney would have differences in EV content. We characterized interstitial EVs from our mouse model using DLS, TRPS, TEM, and Western blot analysis.¹⁵ We determined that both the normal and cystic kidney

papillary lesion. (E, F) Renal cell carcinoma lesions from a 25-week-old *Aqp2CreTsc2^{fl/fl}* mouse. (E) Cystic and solid lesions contain kidney parenchyma (white arrow), renal cell carcinoma (red arrow) and papillary renal cell carcinoma (black arrow). (F) Areas of renal cell carcinoma with rhabdoid features (red arrow). (G) Pax8 staining of adenomatous hyperplasia in a cyst, and (H) the renal cell carcinoma lesion.

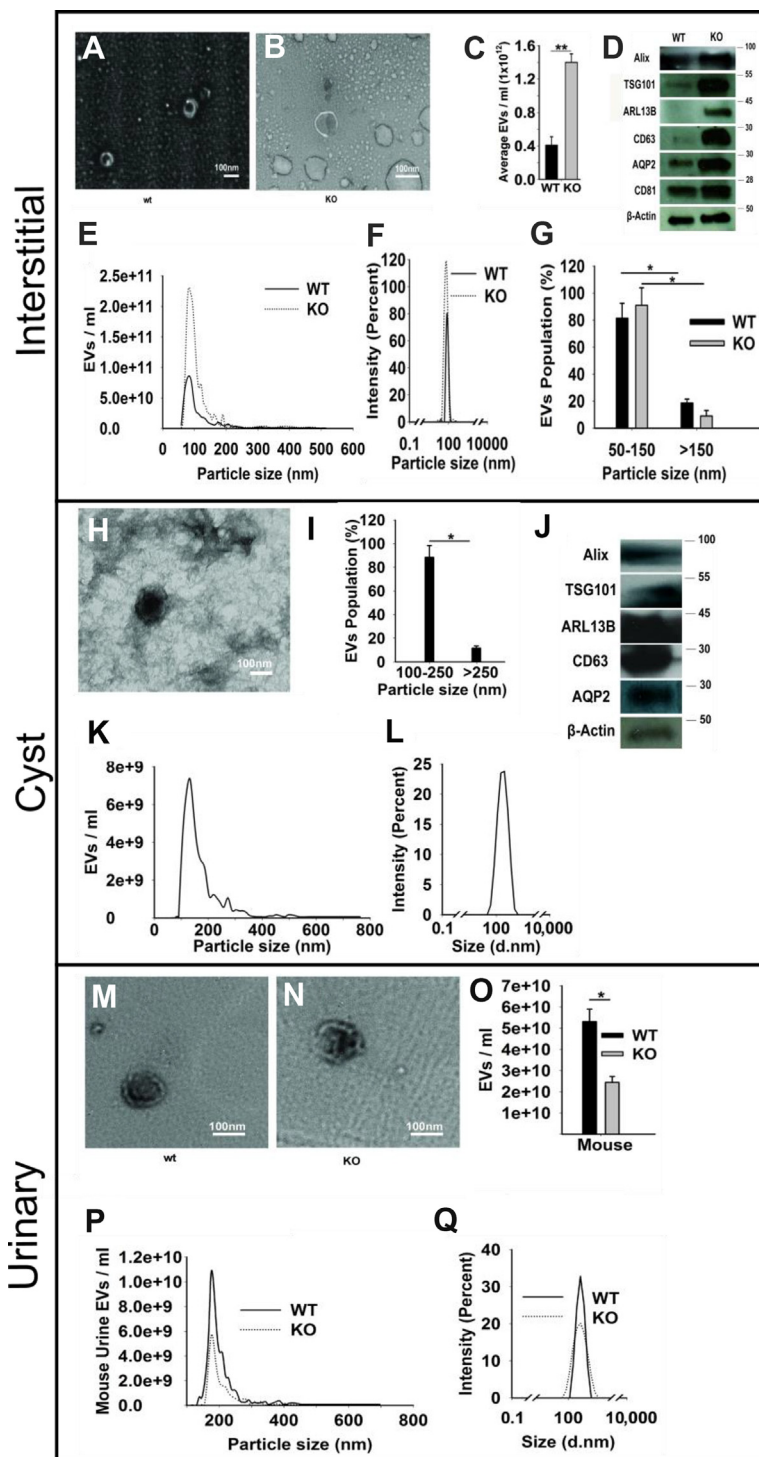


Figure 3 *Tsc2* gene integrity impacts renal EVs (A–G) *Aqp2CreTsc2^{fl/fl}* mouse has more interstitial EVs than normal mouse. (A) TEM of EVs from a wild-type mouse with typical cup-shaped appearance. (B) TEM of EVs from a *Aqp2CreTsc2^{fl/fl}* mouse kidney with the expected morphology. (C) EV abundance histogram for wild-type and *Aqp2CreTsc2^{fl/fl}* mice. (D) Western blot characterizing EVs for signature proteins Alix, TSG101, ARL13B, CD63 and aquaporin-2 with β -actin as loading control. (E) TRPS sizing data. (F) DLS sizing data. (G) Interstitial EV sizing graph. (H–L) Mouse cyst EV characterization. (H) TEM of *Aqp2CreTsc2^{fl/fl}* mouse cyst EVs showing expected morphology. (I) Size profile of cystic EVs. (J) Western blot of cyst EV Alix, TSG101, ARL13B, CD63 and aquaporin-2 with β -actin as loading control. (K) EV sizing by TRPS. (L) EV sizing by DLS. (M–Q) *Aqp2CreTsc2^{fl/fl}* mouse has fewer urinary EVs. (M) TEM of wild-type mouse urinary EVs showing the expected shape. (N) TEM of *Aqp2CreTsc2^{fl/fl}* mouse urinary EVs. (O) EV abundance histogram of urinary EVs by TRPS. (P) Concentration and size of EVs from wild-type and *Aqp2CreTsc2^{fl/fl}* mice. (Q) Wild-type and *Aqp2CreTsc2^{fl/fl}* EV sizing by DLS. Note: Data were presented as Mean \pm SD, $n = 3$ and value of significance expressed as *** $P \leq 0.001$, ** $P \leq 0.01$, * $P \leq 0.05$.

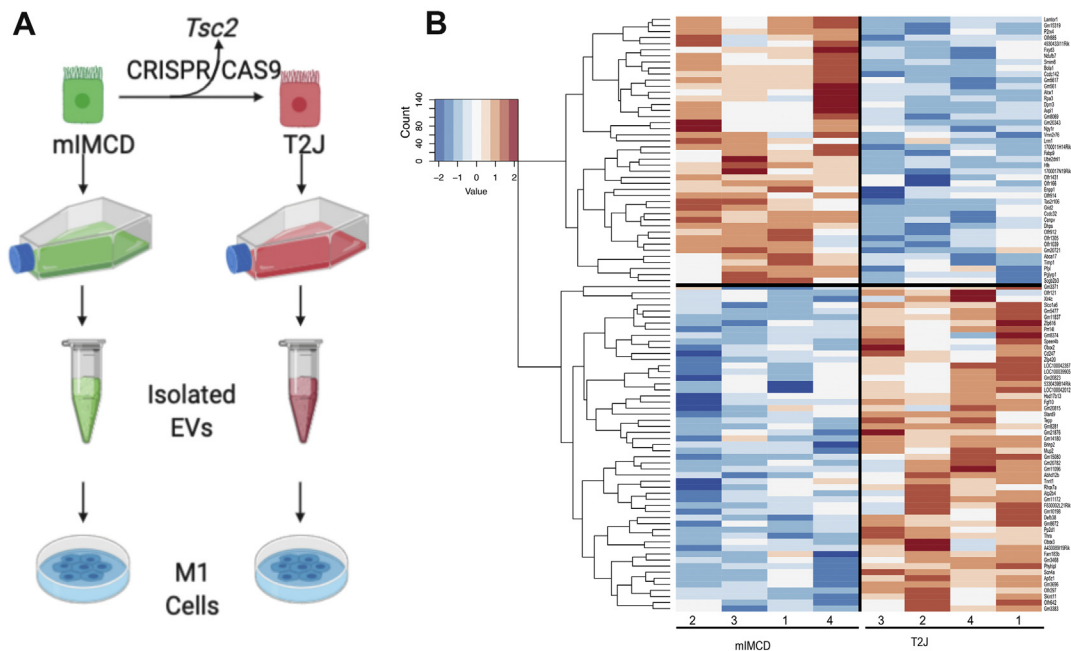


Figure 4 EVs from cells lacking *Tsc2* function alter recipient cell transcriptome. **(A)** Experimental Design. EVs isolated from mIMCD cells with or without a *Tsc2* gene deletion were used to treat M1 cells. **(B)** Microarray data presented as a heatmap of top 100 changes. Note excellent interexperimental agreement.

expressed interstitial EVs of high purity by TEM, as a very high percentage of the structures exhibited the typical cup-shaped morphology (Fig. 3A, B). The cystic kidney expressed at least 4-fold more EVs than the normal kidney (Fig. 3C) when measured by TRPS. On Western blot, the isolated EVs expressed cellular proteins Alix and TSG101; the transmembrane proteins CD63, CD81 and CD9; and the primary cilia-related, Hedgehog signaling-related protein Arl13b. The EVs also expressed the principal cell protein aquaporin-2 (Fig. 3D). All these findings indicated these EVs originated from principal cells. Size agreement was excellent between TEM, TRPS, and DLS (Fig. 3E, F). Interstitial EVs were similar in size at 85–97 nm in diameter (Fig. 3G).

Renal cyst fluid contains abundant EVs

We isolated EVs from mouse cyst fluid using size exclusion chromatography. We performed TRPS, DLS, TEM and Western blot analyses to characterize the EVs within renal cyst fluid from the *Aqp2CreTsc2^{fl/fl}* mouse model.¹⁴ The EVs from mouse cyst fluid demonstrated the expected cup shape (Fig. 3H). The EV size in this population was similar to that found in the interstitial compartment (Fig. 3I). Western blot analyses again revealed the same signature for small EVs as for the interstitial EVs, and cystic EVs also contained aquaporin-2 (Fig. 3J). Sizing by TRPS and DLS (Fig. 3K, L) revealed excellent agreement.

Cystic kidneys excrete fewer urinary EVs than normal kidneys

While the interstitial compartment has more EVs in the diseased kidney and there are EVs in the cyst fluid, we were

curious about urinary EV excretion in the disease state. Both wild-type (WT) and *Aqp2CreTsc2^{fl/fl}* mice had urinary EVs that could be isolated to high purity by TEM (Fig. 3M, N). We detected four-fold fewer urinary EVs (corrected for urinary concentration) from *Aqp2CreTsc2^{fl/fl}* mice than from normal mice (Fig. 3O). There was good agreement for size between TRPS and DLS (Fig. 3P, Q). As expected, the urinary EVs were larger than the interstitial EVs at 166–187 nm.³²

EVs from *Tsc2*-deleted cells alter recipient cell transcriptome to promote secretion and proliferation

To determine the impact of EVs from *Tsc2*-deleted cells on renal collecting duct cells in a well-controlled fashion, we used WT inner medullary collecting duct (IMCD3) and *Tsc2*-deleted (T2J) IMCD3 cells to model principal cells. We have recently published work about these cell lines¹⁴ and have demonstrated that the loss of *Tsc2* gene function significantly increased the production of EVs with an altered proteomic profile.¹⁵ We isolated EVs of these two cell lines, genetically identical except for their *Tsc2* locus, and used the EVs to treat M1 cortical collecting duct cell line cultures for 24 h (Fig. 4A). The M1 cells retain cortical collecting duct cell morphology and antigens and exhibit either intercalated or principal cell characteristics. We found high correlation between the four individual replicates for each experiment in microarray analyses (Fig. 4B) and include to top 26 gene changes and the *P* value for genes effected more so by the EVs from the T2J cell line over the mIMCD cell line EVs, and the top 26 genes effected in a greater fashion by the EVs isolated from the parental mIMCD cell

Table 1 Top 26 induced gene differences.

T2J > mIMCD		mIMCD > T2J	
Gene_Symbol	p value	Gene_Symbol	p value
<i>Dhps</i>	6.09E-05	<i>Pp2d1</i>	2.63E-05
<i>P2rx4</i>	7.03E-05	<i>Thra</i>	6.32E-05
<i>Hfe</i>	1.26E-04	<i>Gm11837</i>	1.25E-04
<i>Gm5617</i>	1.38E-04	<i>Gm3696</i>	1.25E-04
<i>Cenpv</i>	1.42E-04	<i>Olfr297</i>	1.71E-04
<i>Lamtor1</i>	1.78E-04	<i>Gm8281</i>	1.92E-04
<i>Gm15319</i>	1.93E-04	<i>Scn4a</i>	1.95E-04
<i>Bola1</i>	2.32E-04	<i>Gm11172</i>	2.82E-04
<i>Ccdc142</i>	2.50E-04	<i>Ap5z1</i>	3.28E-04
<i>1700011H14Rik</i>	3.30E-04	<i>Gm3468</i>	3.54E-04
<i>Timp1</i>	5.93E-04	<i>Abhd12b</i>	3.65E-04
<i>Pglyrp1</i>	7.00E-04	<i>Brinp2</i>	6.34E-04
<i>Smim8</i>	8.60E-04	<i>Prr14l</i>	7.35E-04
<i>1700017N19Rik</i>	9.71E-04	<i>Speer4b</i>	1.09E-03
<i>Ndufb7</i>	1.10E-03	<i>Fgf10</i>	1.10E-03
<i>Gm8069</i>	1.14E-03	<i>Gm8672</i>	1.12E-03
<i>Gm20721</i>	1.32E-03	<i>Gm3383</i>	1.62E-03
<i>Fabp9</i>	1.68E-03	<i>Zfp420</i>	1.75E-03
<i>Tas2r106</i>	1.85E-03	<i>Skint11</i>	1.95E-03
<i>Gm561</i>	2.10E-03	<i>Mup2</i>	2.10E-03
<i>Grid2</i>	2.12E-03	<i>LOC100039905</i>	2.32E-03
<i>Ube2dnl1</i>	2.54E-03	<i>Olfr642</i>	2.40E-03
<i>Abca17</i>	2.60E-03	<i>Tepp</i>	2.40E-03
<i>Gm20343</i>	2.73E-03	<i>Phyhipl</i>	2.41E-03
<i>Olfr1431</i>	2.84E-03	<i>Gm20782</i>	2.74E-03
<i>Olfr166</i>	3.10E-03	<i>F830002L21Rik</i>	2.78E-03

line over the mutant T2J cell line EVs (Table 1). We compared the M1 cell response to EVs derived from the same cell lines with only the *Tsc2* gene inactivation difference by using the Kyoto Encyclopedia of Genes and Genomes (KEGG) pathway analysis. We examined which pathways were over represented in M1 cells treated with the mIMCD cell-derived EVs compared to those treated with T2J-derived EVs (Table 2). Because the cells were only treated for 24 h with the EVs, we used $P \leq 0.1$ to indicate significance in order to avoid missing interesting findings. The top pathways effected included olfaction transduction, associated with cilia proteins, and several pathways that had interesting gene overlaps. *Enpp1* was significantly increased in the M1 cells treated with EVs derived from the parental mIMCD3 cell line ($P = 0.0082$) as was *RPA3* ($P = 0.0134$). The *Enpp1* gene overlap in the riboflavin metabolism, pantothenate and CoA biosynthetic and starch and sucrose metabolism pathways, and the *RPA3* gene overlaps in the mismatch repair, DNA replication, and double-strand break repair pathways including homologous recombination and nucleoside excision repair.

mTORC1 activity is not the only determinant of EV production

To study the effects of EVs and understand the role of mTORC1 activity in EV-producing cells, we sought methods

Table 2 KEGG Pathway analysis mIMCD Greater than T2J.

KEGG Pathway	p-value
Olfactory transduction	0.01
Riboflavin metabolism	0.02
Pantothenate and CoA biosynthesis	0.04
Neuroactive ligand–receptor interaction	0.04
Mismatch repair	0.05
Starch and sucrose metabolism	0.07
DNA replication	0.07
Nicotinate and nicotinamide metabolism	0.08
Homologous recombination	0.09
Nucleotide excision repair	0.09
Mineral absorption	0.09
ABC transporters	0.10
N-Glycan biosynthesis	0.10

to independently modulate EV production and EV-producing cell mTORC1 activity. mTORC1 is suppressed by hypoxia through a mechanism involving REDD1 releasing TSC2 from the TSC2/14-3-3 complex to lighten mTORC1 repression.³³ Hypoxia is also linked to increased EV production.^{34,35} Hence, we used CoCl_2 , an accepted hypoxia mimetic, in a cell culture model of mTORC1 inhibition.³⁶ Treatment of the cell lines with 100 mM CoCl_2 resulted in a 4-fold ($P < 0.01$) increase in EV production while suppressing mTORC1 activity (Fig. 5A, B). Because of the media change, the pS6 kinase phosphorylation in mIMCD was also robust. LiCl treatment interferes with glycogen synthase kinase 3 (GSK3) repression of *Tsc2*, which is associated with cystic disease^{37–39} that is prevented by mTORC1 inhibition.⁴⁰ Thus, we assessed the effect of LiCl on EV production and cellular mTORC1 activity. We found that LiCl stimulates mTORC1 activity but did not change EV production in EV-producing cells (Fig. 5C, D).

Inhibiting mTORC1 activity is safe in mice¹⁴ and humans^{41,42} and can shrink renal angiomyolipomata. Therefore, we examined the *in vitro* effect of rapamycin, an mTORC1 inhibitor, on EV production and activity. Using Western blot analysis, we found that treating M1 cells with rapamycin reduced mTORC1 activity (S6 phosphorylation) upon EV-treatment. Treating EV-producing cells with rapamycin significantly changed the effects of EVs isolated from both the WT and *Tsc2* mutant (Fig. 5E). The mTORC1 inhibition was ‘transferred’ to recipient M1 cells via EVs produced by *Tsc2*-deleted T2J cells but not from mIMCD cells (Fig. 5E). mTORC1 inhibition also significantly reduced EV production in both WT and *Tsc2* mutant cell lines (Fig. 5F). We posited that mTORC1 inhibition may also reduce *in vivo* EV production, which may be part of the drug mechanism of action. To test this, we treated WT and *Aqp2CreTsc2^{fl/fl}* mice with rapamycin and compared the interstitial EV numbers to untreated group controls (Fig. 5G). Rapamycin reduced interstitial EVs by 30% ($P < 0.05$). Furthermore, rapamycin reduced the EV concentration back to WT levels, and rapamycin treatment did not affect the EV concentration in WT kidneys. Even though a large renal cyst is a closed system,⁴³ we found that after

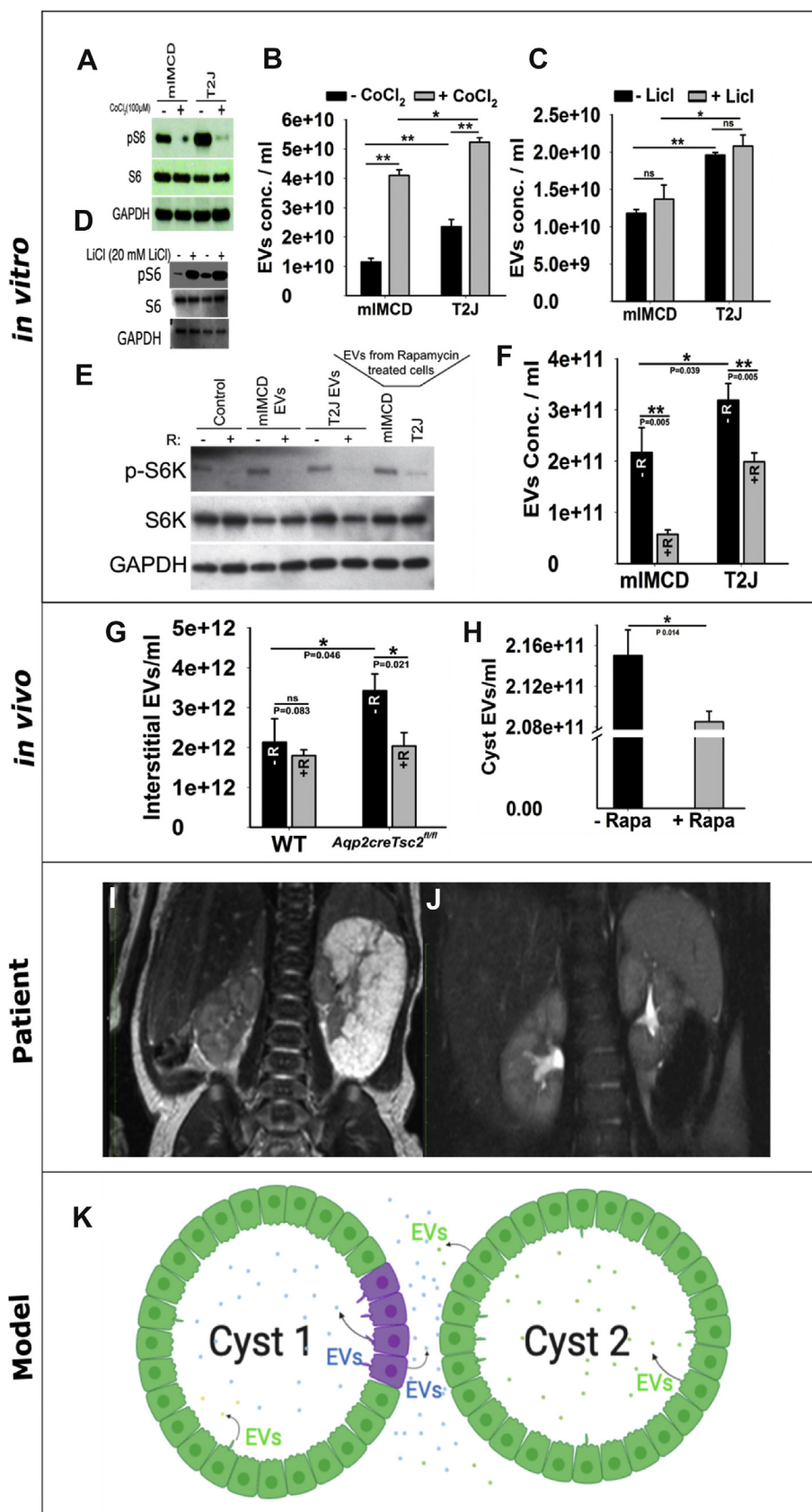


Figure 5 (A–F) EV production is independent of mTORC1 activity in the producing cell. (A) Western blot for pS6 activity for following CoCl₂ exposure. Cells were more actively growing such that IMCD cells had a more robust pS6 signal. (B) Analysis of the concentration of the isolated EVs. (C) EV concentration analysis for LiCl-treated cells. (D) Western blot for pS6 activity for following

just 14 days, the cystic fluid EV concentration was reduced (Fig. 5H). These effects on mTORC1 activity and EVs correlate well with patient therapy. When cysts are small, they can be induced to shrink below the resolution of clinical MRI scanning by prolonged use of an mTORC1 inhibitor^{14,44} (Fig. 5I, J).

Discussion

We describe a cell nonautonomous disease trait mediated by *Tsc2*-deficient renal epithelial cell derived EVs that reprogram genetically intact epithelial cells to adopt the disease phenotype (Fig. 5K). The accepted molecular pathogenesis of TSC renal disease, based on findings in angiomyolipomata, involves a 'second hit' at the involved TSC locus,⁴⁵ and is supported by the loss of the TSC protein.⁴⁶ This second hit mechanism is difficult to reconcile with murine *Tsc* cystic disease because we failed to find somatic mutations in a majority of cysts, indicating that the majority of renal cysts maintain their *Tsc* locus integrity.^{47,48} Human TSC cysts continue to express both tuberin and hamartin.⁴⁹ Although a role for EVs is recognized in development and renal pathophysiological functions,^{26,50} this is the first evidence that EVs play a role in TSC renal cystic disease. We posit that the cells that did undergo the second somatic mutation produce EVs that reprogram genetically intact cells to proliferate and secrete fluid, resulting in the cystic phenotype.

Using our novel mouse models, we identified cysts with a range of principal cell lineage contributions (Fig. 1A). This range is due to a sampling issue because cysts are three-dimensional structures but histologically we only see a two-dimension representation. In most cysts, we at least find rare principal cells by DBA staining. These DBA results correlate well with the fluorescence data obtained using the *Aqp2CreTsc2^{fl/fl}Confetti* mouse model, where we find a range of fluorescence by lineage tracing. We identified clonal expansion based on the fluorescence of the recombined principal cells (Fig. 1C, E–I). We also determined that both recombined principal cells (fluorescent) and genetically intact cells (not fluorescent) contributed to papillary tumors. The cysts and papillary structures are the result of a somewhat slow but relentless growth process (Fig. 2), as is appreciated for the human disease. The Pax8 expression in these proliferative lesions (Fig. 2G and H) supports that lesions arose from the collecting duct.

To discern the mechanism for genetically intact cells behaving as *Tsc2*-mutant cells, we investigated the role of EVs. We found a significant increase in interstitial EVs in the mutant kidney (Fig. 3A–G). Renal cystic disease is associated with changes in blood flow and hypoxia,⁵¹ and hypoxia is a powerful stimulus for EV production.^{34,52} The urinary excretion of EVs was significantly reduced, even when we corrected for urine osmolality (Fig. 3P). This may be due to a change in the polarity of EV secretion from luminal to basolateral secretion or that the EVs that would otherwise be in the urine are trapped in the cysts (Fig. 3H–L).

To determine if EVs could reprogram renal epithelial cells, we developed a cell culture model. We used this approach because there may be several stages in the development of renal cystic disease and understanding the initial phase in an *in vivo* model would have an inherent risk of contamination from surrounding cysts at different stages. We used a mIMCD cell line and disrupted the *Tsc2* gene using CRISPR/CAS9 (Fig. 4A). This approach ensured the cells were isogenic except for the *Tsc2* gene. The isolated EVs had consistent and significantly different effects on the target M1 renal tubular cell line (Fig. 4B). The M1 cells exposed to EVs from mIMCD cell EVs exhibited more DNA repair pathway proteins than when exposed to EVs from T2J cells, likely resulting from adaptation to the oxidative pressure of cell culture. The finding that the *Enpp1* gene was down-regulated in the M1 cells treated from the *Tsc2* mutant T2J cells was interesting for two major reasons. First, the regulation must presumably be due to miRNA and lncRNA cargo, and second, this gene is known to be suppressed by increased mTORC1 activity.⁵³

Transcriptomic profiling showed that EVs from the *Tsc2*-mutant cell line caused M1 cells to adopt a more secretory phenotype and exhibit more proliferative processes. This phenotype is logical for the changes necessary for a normally absorptive cell to become secretory and proliferate to form a cyst. Because intercalated cells use H⁺-ATPase to energize transport processes⁵⁴ and there is such plasticity in the collecting duct, it is possible that EVs induce all the cells in the cyst, principal and intercalated, to upregulate H⁺-ATPase to facilitate fluid excretion in cyst formation.

The role of H⁺-ATPase and the cyst distribution in the *Aqp2CreTsc2^{fl/fl}* model¹⁴ may offer a hint toward therapy. The TSC cystic disease is cortically restricted. It is possible that there is a EV intercellular polarity such that principal cells communicate to the intercalated cells to form cysts. However, the same effect does not

LiCl exposure. (E–J) Effect of mTORC1 inhibition on EV effects and production. (E) Lane 1 to 6, we treated M1 cells for 24 h with EVs from cells treated with and without 100 nM rapamycin. Control group not treated with EVs. Lane 7&8: M1 cell lysate treated with EVs of 24 h rapamycin-treated mIMCD and T2J cells. (F) Rapamycin reduces EV production in mIMCD cells ($P < 0.01$) and T2J cells ($P < 0.05$). (G, H) Rapamycin decreases interstitial (G) and cyst (H) EV production *in vivo*. *Aqp2CreTsc2^{fl/fl}* and wild-type (WT) mice. Mice were interperitoneally injected with vehicle solution or rapamycin (1 mg/kg) for two weeks, twice a week. After completion, interstitial and cyst fluid EVs were isolated and quantitated. (I) Coronal MRI of a six-month-old with cortical cystic proliferative lesion. (J) Same infant at 18 months after one year of treatment with mTORC1 inhibitor. (K) EVs and *Tsc* cystic disease. Cysts are comprised of non-mutant cells (green) with fewer *Tsc2*-mutant, clonally expanded cells (purple). More abundant and altered EVs from these *Tsc*-deleted tubular epithelial cells induce cell proliferation and fluid secretion, resulting in the disease phenotype. The communication may be intraluminal (Cyst 1) or through the interstitial space (Cyst 2). Note: Data were presented as Mean \pm SD, $n = 3$ and value of significance expressed as *** $P \leq 0.001$, ** $P \leq 0.01$, * $P \leq 0.05$. Abbreviation: –R or –Rapa: Not treated with Rapamycin; +R or + Rapa: Treated with Rapamycin.

occur when principal cells are much more abundant and the intercalated cells are much less present, such as in the renal medulla. Given the cellular plasticity between principal cells and intercalated cells, one possible form of therapy may be to shift the collecting duct cells toward principal cells, for example, using a carbonic acid anhydrase inhibitor.

We found that increased mTORC1 activity correlated with EV production, wanted to determine if this was a fixed correlation or if there were conditions in which the EV concentration and mTORC1 activity in EV-producing cells differed. Because hypoxia stimulates EV production, we used the hypoxia mimetic CoCl_2 to treat our cells. CoCl_2 significantly increased EV production while significantly reducing mTORC1 activity in treated cells. Although the Tsc2 protein is involved in the hypoxia suppression of mTORC1 in mouse embryonic fibroblasts,^{55,56} the duration of hypoxia mimetic exposure and the cell type are different and reveal that there is a more complex regulation at play. The key finding of this experiment is that mTORC1 activity in EV-producing cells is not the only regulator of EV production. Complementing this finding, LiCl treatment increased mTORC1 activity in EV-producing cells but did not increase EV production (Fig. 5A–D), further supporting the possibility that the EV cargo may be very different depending on the conditions, and that the effect may not be only dependent on the number of EVs. mTORC1 inhibition reduced the mTORC1 activity and EV production in the treated cell. EVs from Tsc2-mutant cells that were treated with rapamycin also suppressed mTORC1 activity in the recipient M1 cell line (Fig. 5E). After two weeks of mTORC1 inhibition *in vivo*, the mouse cystic kidney interstitial EV concentration was significantly lower than WT concentrations (Fig. 5G). This large effect was likely due to turnover in the interstitial space, in part by lymphatic clearance. Even after only two weeks of treatment, the cystic fluid EVs of rapamycin-treated animals were less concentrated than those of untreated animals (Fig. 5H). This may be how mTORC1 inhibitors reduce the human cystic disease burden when small cysts that still communicate with the rest of the tubule are treated (Fig. 5I, J). The impact of mTORC1 inhibition on EV production and cargo may be a critical component of how mTORC1 inhibition translates into a therapy for TSC renal disease.

Tsc2 is not the only tumor suppressor gene that exhibits such a cell nonautonomous influence on surrounding cells. A similar effect has been described for the breast cancer type 1 (BRCA1) susceptibility gene. In patients with germline BRCA1 mutations, many tumors demonstrate loss of heterozygosity at the BRCA1 locus and the retention of the mutant allele,^{57–59} suggesting that BRCA1 may act as a classical tumor suppressor. However, not all tumors exhibit losses of heterozygosity at this locus,⁵⁷ and there is little convincing evidence that the WT allele in these tumors is silenced by epigenetic mechanisms.⁶⁰ To better understand the role of BRCA1 in gynecological malignancy, Chodankar et al used a Cre-lox system to inactivate Brca1 in mouse ovarian granulosa cells by using a truncated form of the Fsh receptor promoter to drive Cre recombinase.⁶¹ The authors demonstrated that inactivation of the Brca1 gene in granulosa cells led to the development of cystic tumors with genetically intact Brca1 genes in the ovaries and uterine

horns. They posited that the loss of Brca1 may influence tumor development indirectly, through some form of effector secreted by granulosa cells. Given our results, we posit that EVs are the secreted effector. This may be more generalizable such that EV-mediated cellular reprogramming also may be involved in other tumor suppressor gene-related tumors.

Conclusions

Our studies support a cell nonautonomous effect driven by EVs, that conscripts genetically intact cells into cystic and even renal cancer phenotypes. These findings indicate that changing EV communication may provide a new therapeutic target for TSC renal cystic disease and possibly some cancers. Understanding this biology may have important implications for the renal cell carcinoma phenotype. For TSC cystic disease, altering this EV communication early might offer great promise to prolong renal function.

Author contributions

Conceptualization, F.Z., J.J.B., P.K. and Y.Y.; Methodology, F.Z., J.J.B., P.K. and Y.Y.; Investigation, F.Z., J.J.B., P.K. and Y.Y.; Resources, B.S.; J.J.B.; Data Curation F.Z., J.J.B., P.K. and Y.Y.; Writing – Original Draft Preparation, A.A., F.Z., J.J.B., K.W.G. P.K. and Y.Y.; Writing – Review & Editing, A.A., F.Z., J.J.B., K.W.G. P.K.; Supervision, J.J.B.; Funding Acquisition. J.J.B.

Conflict of interests

The authors declare no conflict of interest.

Funding

This work was supported by DoD (No. W81XWH-14-1-0343) (JJB), Federal Express Chair of Excellence (JJB), and Children's Foundation Research Institute (JJB).

References

1. Little M, Georgas K, Pennisi D, Wilkinson L. Kidney development: two tales of tubulogenesis. *Curr Top Dev Biol.* 2010;90:193–229.
2. Eladari D, Chambrey R, Peti-Peterdi J. A new look at electrolyte transport in the distal tubule. *Annu Rev Physiol.* 2012;74:325–349.
3. Wall SM. Recent advances in our understanding of intercalated cells. *Curr Opin Nephrol Hypertens.* 2005;14(5):480–484.
4. Al-Awqati Q, Gao XB. Differentiation of intercalated cells in the kidney. *Physiology (Bethesda).* 2011;26(4):266–272.
5. Breton S, Alper SL, Gluck SL, Sly WS, Barker JE, Brown D. Depletion of intercalated cells from collecting ducts of carbonic anhydrase II-deficient (CAR2 null) mice. *Am J Physiol.* 1995;269(6 Pt 2):F761–F774.
6. Jeong HW, Jeon US, Koo BK, et al. Inactivation of Notch signaling in the renal collecting duct causes nephrogenic diabetes insipidus in mice. *J Clin Invest.* 2009;119(11):3290–3300.
7. Christensen BM, Marples D, Kim YH, Wang W, Frøkiær J, Nielsen S. Changes in cellular composition of kidney collecting duct cells in

- rats with lithium-induced NDI. *Am J Physiol Cell Physiol.* 2004;286(4):C952–C964.
8. Kim WY, Nam SA, Choi A, et al. Aquaporin 2-labeled cells differentiate to intercalated cells in response to potassium depletion. *Histochem Cell Biol.* 2016;145(1):17–24.
 9. Ma M, Jiang YJ. Jagged2a-notch signaling mediates cell fate choice in the zebrafish pronephric duct. *PLoS Genet.* 2007;3(1):e18.
 10. Blomqvist SR, Vidarsson H, Fitzgerald S, et al. Distal renal tubular acidosis in mice that lack the forkhead transcription factor Foxo1. *J Clin Invest.* 2004;113(11):1560–1570.
 11. Guo Q, Wang Y, Tripathi P, et al. Adam10 mediates the choice between principal cells and intercalated cells in the kidney. *J Am Soc Nephrol.* 2015;26(1):149–159.
 12. Street JM, Birkhoff W, Menzies RI, Webb DJ, Bailey MA, Dear JW. Exosomal transmission of functional aquaporin 2 in kidney cortical collecting duct cells. *J Physiol.* 2011;589(Pt 24):6119–6127.
 13. Oosthuyzen W, Scullion KM, Ivy JR, et al. Vasopressin regulates extracellular vesicle uptake by kidney collecting duct cells. *J Am Soc Nephrol.* 2016;27(11):3345–3355.
 14. Bissler JJ, Zadjali F, Bridges D, et al. Tuberous sclerosis complex exhibits a new renal cystogenic mechanism. *Physiol Rep.* 2019;7(2):e13983.
 15. Zadjali F, Kumar P, Yao Y, et al. Tuberous sclerosis complex axis controls renal extracellular vesicle production and protein content. *Int J Mol Sci.* 2020;21(5):1729.
 16. Snippert HJ, van der Flier LG, Sato T, et al. Intestinal crypt homeostasis results from neutral competition between symmetrically dividing Lgr5 stem cells. *Cell.* 2010;143(1):134–144.
 17. Wu D, Yotnda P. Induction and testing of hypoxia in cell culture. *J Vis Exp.* 2011;54:2899.
 18. Price KL, Kolatsi-Joannou M, Mari C, Long DA, Winyard PJD. Lithium induces mesenchymal-epithelial differentiation during human kidney development by activation of the Wnt signalling system. *Cell Death Discov.* 2018;4:13.
 19. Fingar DC, Salama S, Tsou C, Harlow E, Blenis J. Mammalian cell size is controlled by mTOR and its downstream targets S6K1 and 4EBP1/eIF4E. *Genes Dev.* 2002;16(12):1472–1487.
 20. Holthöfer H, Schulte BA, Spicer SS. Expression of binding sites for Dolichos biflorus agglutinin at the apical aspect of collecting duct cells in rat kidney. *Cell Tissue Res.* 1987;249(3):481–485.
 21. Assmus AM, Mansley MK, Mullins LJ, Peter A, Mullins JJ. mCCD c1 cells show plasticity consistent with the ability to transition between principal and intercalated cells. *Am J Physiol Renal Physiol.* 2018;314(5):F820–F831.
 22. Lai CPT, Yeong JPS, Tan AS, et al. Evaluation of phospho-histone H3 in Asian triple-negative breast cancer using multiplex immunofluorescence. *Breast Cancer Res Treat.* 2019;178(2):295–305.
 23. Kim JY, Jeong HS, Chung T, et al. The value of phosphohistone H3 as a proliferation marker for evaluating invasive breast cancers: a comparative study with Ki67. *Oncotarget.* 2017;8(39):65064–65076.
 24. Khieu ML, Broadwater DR, Aden JK, Coviello JM, Lynch DT, Hall JM. The utility of phosphohistone H3 (PHH3) in follicular lymphoma grading: a comparative study with ki-67 and H&E mitotic count. *Am J Clin Pathol.* 2019;151(6):542–550.
 25. McGough IJ, Vincent JP. Exosomes in developmental signalling. 2016;143(14):2482–2493.
 26. Pomatto MAC, Gai C, Bussolati B, Camussi G. Extracellular vesicles in renal pathophysiology. *Front Mol Biosci.* 2017;4:37.
 27. Lv LL, Feng TT, Liu BC. New insight into the role of extracellular vesicles in kidney disease. *J Cell Mol Med.* 2019;23(2):731–739.
 28. Becker A, Thakur BK, Weiss JM, Kim HS, Peinado H, Lyden D. Extracellular vesicles in cancer: cell-to-cell mediators of metastasis. *Cancer Cell.* 2016;30(6):836–848.
 29. Grange C, Collino F, Tapparo M, Camussi G. Oncogenic micro-RNAs and renal cell carcinoma. *Front Oncol.* 2014;4:49.
 30. van Balkom BWM, Pisitkun T, Verhaar MC, Knepper MA. Exosomes and the kidney: prospects for diagnosis and therapy of renal diseases. *Kidney Int.* 2011;80(11):1138–1145.
 31. Grange C, Tapparo M, Collino F, et al. Microvesicles released from human renal cancer stem cells stimulate angiogenesis and formation of lung premetastatic niche. *Cancer Res.* 2011;71(15):5346–5356.
 32. Musante L, Bontha SV, La Salvia S, et al. Rigorous characterization of urinary extracellular vesicles (uEVs) in the low centrifugation pellet - a neglected source for uEVs. *Sci Rep.* 2020;10(1):3701.
 33. Nikiforova NV, Kirpatovskii VI, Chumakov AM, Darenkov AF. Content of vitamins E and A in tumor tissue in kidney cancer. *Biull Eksp Biol Med.* 1993;115(3):290–293.
 34. Zhang G, Yang Y, Huang Y, et al. Hypoxia-induced extracellular vesicles mediate protection of remote ischemic preconditioning for renal ischemia-reperfusion injury. *Biomed Pharmacother.* 2017;90:473–478.
 35. Kilic T, Valinhas ATS, Wall I, Renaud P, Carrara S. Label-free detection of hypoxia-induced extracellular vesicle secretion from MCF-7 cells. *Sci Rep.* 2018;8(1):9402.
 36. Muñoz-Sánchez J, Cháñez-Cárdenas ME. The use of cobalt chloride as a chemical hypoxia model. *J Appl Toxicol.* 2019;39(4):556–570.
 37. Farres MT, Ronco P, Saadoun D, et al. Chronic lithium nephropathy: MR imaging for diagnosis. *Radiology.* 2003;229(2):570–574.
 38. Wood CG 3rd, Stromberg LJ 3rd, Harmath CB, et al. CT and MR imaging for evaluation of cystic renal lesions and diseases. *Radiographics.* 2015;35(1):125–141.
 39. Khan M, El-Mallakh RS. Renal microcysts and lithium. *Int J Psychiatry Med.* 2015;50(3):290–298.
 40. Gao Y, Romero-Aleshire MJ, Cai Q, Price TJ, Brooks HL. Rapamycin inhibition of mTORC1 reverses lithium-induced proliferation of renal collecting duct cells. *Am J Physiol Renal Physiol.* 2013;305(8):F1201–F1208.
 41. Bissler JJ, McCormack FX, Young LR, et al. Sirolimus for angiomyolipoma in tuberous sclerosis complex or lymphangioleiomyomatosis. *N Engl J Med.* 2008;358(2):140–151.
 42. Bissler JJ, Kingswood JC, Radzikowska E, et al. Everolimus for angiomyolipoma associated with tuberous sclerosis complex or sporadic lymphangioleiomyomatosis (EXIST-2): a multicentre, randomised, double-blind, placebo-controlled trial. *Lancet.* 2013;381(9869):817–824.
 43. Grantham JJ, Geiser JL, Evan AP. Cyst formation and growth in autosomal dominant polycystic kidney disease. *Kidney Int.* 1987;31(5):1145–1152.
 44. Siroky BJ, Towbin AJ, Trout AT, et al. Improvement in renal cystic disease of tuberous sclerosis complex after treatment with mammalian target of rapamycin inhibitor. *J Pediatr.* 2017;187:318–322.
 45. Lam HC, Nijmeh J, Henske EP. New developments in the genetics and pathogenesis of tumours in tuberous sclerosis complex. *J Pathol.* 2017;241(2):219–225.
 46. Giannikou K, Malinowska IA, Pugh TJ, et al. Whole exome sequencing identifies TSC1/TSC2 biallelic loss as the primary and sufficient driver event for renal angiomyolipoma development. *PLoS Genet.* 2016;12(8):e1006242.
 47. Onda H, Lueck A, Marks PW, Warren HB, Kwiatkowski DJ. Tsc2(+/-) mice develop tumours in multiple sites that express gelsolin and are influenced by genetic background. *J Clin Invest.* 1999;104(6):687–695.

48. Wilson C, Bonnet C, Guy C, et al. Tsc1 haploinsufficiency without mammalian target of rapamycin activation is sufficient for renal cyst formation in Tsc1^{+/-} mice. *Cancer Res.* 2006; 66(16):7934–7938.
49. Bonsib SM, Boils C, Gokden N, et al. Tuberous sclerosis complex: hamartin and tuberlin expression in renal cysts and its discordant expression in renal neoplasms. *Pathol Res Pract.* 2016;212(11):972–979.
50. Nonaka S, Shiratori H, Saijoh Y, Hamada H. Determination of left-right patterning of the mouse embryo by artificial nodal flow. *Nature.* 2002;418(6893):96–99.
51. Theodorakopoulou M, Raptis V, Loutradis C, Sarafidis P. Hypoxia and endothelial dysfunction in autosomal-dominant polycystic kidney disease. *Semin Nephrol.* 2019;39(6):599–612.
52. Zonneveld MI, Keulers TGH, Rouschop KMA. Extracellular vesicles as transmitters of hypoxia tolerance in solid cancers. *Cancers (Basel).* 2019;11(2):154.
53. Panda DK, Bai X, Sabbagh Y, et al. Defective interplay between mTORC1 activity and endoplasmic reticulum stress-unfolded protein response in uremic vascular calcification. *Am J Physiol Renal Physiol.* 2018;314(6):F1046–F1061.
54. Chambrey R, Kurth I, Peti-Peterdi J, et al. Renal intercalated cells are rather energized by a proton than a sodium pump. *Proc Natl Acad Sci U S A.* 2013;110(19):7928–7933.
55. Deyoung MP, Horak P, Sofer A, Sgroi D, Ellisen LW. Hypoxia regulates TSC1/2-mTOR signaling and tumor suppression through REDD1-mediated 14-3-3 shuttling. *Genes Dev.* 2008; 22(2):239–251.
56. Brugarolas J, Lei K, Hurley RL, et al. Regulation of mTOR function in response to hypoxia by REDD1 and the TSC1/TSC2 tumor suppressor complex. *Genes Dev.* 2004;18(23):2893–2904.
57. Neuhausen SL, Marshall CJ. Loss of heterozygosity in familial tumors from three BRCA1-linked kindreds. *Cancer Res.* 1994; 54(23):6069–6072.
58. Cornelis RS, Neuhausen SL, Johansson O, et al. High allele loss rates at 17q12-q21 in breast and ovarian tumors from BRCA1-linked families. The Breast Cancer Linkage Consortium. *Genes Chromosomes Cancer.* 1995;13(13):203–210.
59. Smith SA, Easton DF, Evans DG, Ponder BA. Allele losses in the region 17q12–21 in familial breast and ovarian cancer involve the wild-type chromosome. *Nat Genet.* 1992;2(2):128–131.
60. Esteller M, Silva JM, Dominguez G, et al. Promoter hypermethylation and BRCA1 inactivation in sporadic breast and ovarian tumors. *J Natl Cancer Inst.* 2000;92(7):564–569.
61. Chodankar R, Kwang S, Sangiorgi F, et al. Cell-nonautonomous induction of ovarian and uterine serous cystadenomas in mice lacking a functional Brca1 in ovarian granulosa cells. *Curr Biol.* 2005;15(6):561–565.